Nonmuscle myosin II exerts tension but does not translocate actin in vertebrate cytokinesis

Xuefei Ma[a,1], Mihály Kovács[b,1], Mary Anne Conti[a], Aibing Wang[a], Yingfan Zhang[a], James R. Sellers[c], and Robert S. Adelstein[a,2]

[a]Laboratory of Molecular Cardiology, National Heart, Lung, and Blood Institute, National Institutes of Health, Bethesda, MD 20892; [b]Department of Biochemistry, Eötvös Loránd University–Hungarian Academy of Sciences "Momentum" Motor Enzymology Research Group, Eötvös University, H-1117 Budapest, Hungary; and [c]Laboratory of Molecular Physiology, National Heart, Lung, and Blood Institute, National Institutes of Health, Bethesda, MD 20892

Edited by Douglas Robinson, The John Hopkins University School of Medicine, Baltimore, MD, and accepted by the Editorial Board February 13, 2012 (received for review October 3, 2011)

During vertebrate cytokinesis it is thought that contractile ring constriction is driven by nonmuscle myosin II (NM II) translocation of antiparallel actin filaments. Here we report in situ, in vitro, and in vivo observations that challenge this hypothesis. Graded knockdown of NM II in cultured COS-7 cells reveals that the amount of NM II limits ring constriction. Restoration of the constriction rate with motor-impaired NM II mutants shows that the ability of NM II to translocate actin is not required for cytokinesis. Blebbistatin inhibition of cytokinesis indicates the importance of myosin strongly binding to actin and exerting tension during cytokinesis. This role is substantiated by transient kinetic experiments showing that the load-dependent mechanochemical properties of mutant NM II support efficient tension maintenance despite the inability to translocate actin. Under loaded conditions, mutant NM II exhibits a prolonged actin attachment in which a single mechanoenzymatic cycle spans most of the time of cytokinesis. This prolonged attachment promotes simultaneous binding of NM II heads to actin, thereby increasing tension and resisting expansion of the ring. The detachment of mutant NM II heads from actin is enhanced by assisting loads, which prevent mutant NM II from hampering furrow ingression during cytokinesis. In the 3D context of mouse hearts, mutant NM II-B R709C that cannot translocate actin filaments can rescue multinucleation in NM II-B ablated cardiomyocytes. We propose that the major roles of NM II in vertebrate cell cytokinesis are to bind and cross-link actin filaments and to exert tension on actin during contractile ring constriction.

cortical tension | myosin II kinetics | graded myosin knockdown | motor-impaired myosin | myosin–actin binding

In vertebrate cells, nonmuscle myosin II (NM II) and cytoplasmic actin are the two major contractile proteins mediating cytokinesis, the process by which one cell divides into two. The three NM II paralogs (II-A, II-B, and II-C) are composed of catalytically active heads, which bind to and translocate actin in an ATP-dependent manner, and bipolar filament-forming rods (1). Current concepts of vertebrate cytokinesis favor the notion of translocation of actin filaments by NM II motors to effect cell division (2–6). Translocation is linked to the hydrolysis of MgATP, resulting in conversion of chemical energy into mechanical movement. In cytokinesis, this movement was thought to be manifested by the sliding of actin filaments by bipolar filaments of NM II to form a narrow contractile ring in the cell's center that ultimately pinches closed to form two new cells.

Previous experiments demonstrated that the three paralogs of vertebrate NM II differ in their heavy chains (NMHCs), which are the products of three different genes, but share the same two pairs of light chains (1). Each NM II has a unique enzymatic activity (rate of MgATP hydrolysis) and duty ratio (the fraction of time that the myosin molecule remains bound to actin during a contractile cycle). Previous work has demonstrated that a reduction of NM II-B in COS-7 cells by siRNA treatment results in multinucleation reflecting a defect in cytokinesis but not in karyokinesis. Multinucleation in siRNA-treated COS-7 cells can be rescued by the transfection of any of the three NM II paralogs (7). Although this result is not surprising, we present here a set of experiments that challenge the present idea that cytokinesis requires the translocation of actin filaments by NM II. Using a combination of in situ (COS-7 cells treated with siRNA and blebbistatin), kinetic (stopped-flow experiments with baculovirus-expressed protein), and in vivo (genetically altered cardiomyocytes in mouse hearts) approaches, we provide evidence that it is the binding of myosin to actin as well as the tension that is exerted on the actin filaments by NM II that is critical for cells to divide.

Results

Motor-Impaired NM IIs Support Cytokinesis in Cultured COS-7 Cells. Previous work has shown that depleting the major NM II paralog, NMHC II-B, in COS-7 cells resulted in multinucleation due to a failure in cytokinesis and that this defect of cytokinesis could be successfully rescued by exogenous expression of NMHC II-A, II-B, or II-C (7). To address whether NM II actin translocation is essential during COS-7 cell cytokinesis, motor-impaired NM IIs were expressed in COS-7 cells following siRNA knockdown of NMHC II-B. Fig. 1 *A* and *B* shows that multinucleation in COS-7 cells can be prevented by expressing mutant forms of NM II-B (GFP-NMHC II-B R709C) or NM II-A (GFP-NMHC II-A N93K). These two mutant NM IIs, which were assayed in vitro as heavy meromyosin (HMM) fragments, have previously been shown to have marked reductions in actin-activated MgATPase activities and no detectable ability to translocate actin filaments in vitro although both mutant NM IIs can bind to actin and be released by MgATP (8, 9). Recently, we have expressed the NM II-B R709C mutant as a full-length molecule using baculovirus expression and have substantiated its inability to translocate actin filaments using an in vitro motility assay in the presence of 150 mM KCl (Table S1). Importantly, these mutations in vivo have been shown to cause major abnormalities in both humans [NM II-A (10)] and mice [NM II-B (11)]. Seventy-two hours following knockdown of NMHC II-B by siRNA, COS-7 cells expressing the mutant NM IIs are mononucleated (Fig. 1 *A* and *B*, arrowheads), but those with no mutant NM II expression remain multinucleated (Fig. 1 *A* and *B*, arrows). Fig. 1*B* also shows that GFP-NM II-A N93K localizes to the cleavage furrow of a dividing COS-7 cell (arrowhead). Fig. 1*C* provides quantification of the rescue of multinucleation in COS-7 cells. The ability of the motor-impaired NM IIs to rescue cytokinesis raises the possibility that the role of NM II in cytokinesis is not dependent on its enzymatic motor activity to effect translocation of actin filaments.

Author contributions: X.M., M.K., and R.S.A. designed research; X.M., M.K., M.A.C., and J.R.S. performed research; A.W. and Y.Z. contributed new reagents/analytic tools; X.M., M.K., and J.R.S. analyzed data; and X.M., M.K., M.A.C., and R.S.A. wrote the paper.

The authors declare no conflict of interest.

This article is a PNAS Direct Submission. D.R. is a guest editor invited by the Editorial Board.

[1]X.M. and M.K. contributed equally to this work.

[2]To whom correspondence should be addressed. E-mail: adelster@nhlbi.nih.gov.

This article contains supporting information online at www.pnas.org/lookup/suppl/doi:10.1073/pnas.1116268109/-/DCSupplemental.

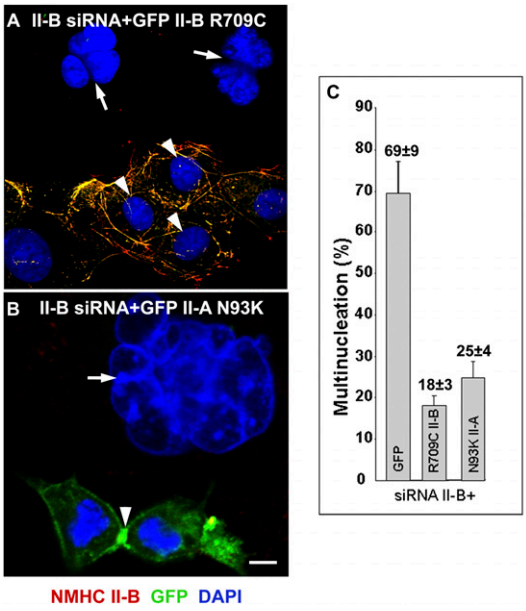

Fig. 1. Immunofluorescence confocal microscope images of cultured COS-7 cells stained with NMHC II-B antibodies (*A*, red; yellow due to merge of antibody staining and GFP-NM II-B) 72 h following transfection with GFP-NMHC II-B R709C during NMHC II-B siRNA treatment. Cells become multinucleated due to loss of NM II-B (*A*, arrows) but are mononucleated in the presence of GFP-NMHC II-B R709C (*A*, arrowheads). (*B*) Mononucleation is also restored by transfection with GFP-NMHC II-A N93K, which localizes to the contractile ring of a dividing cell (*B*, green, arrowhead). Untransfected cells remain multinucleated (*A* and *B*, arrows). DAPI (blue) stains nuclei. (*C*) Quantitation of multinucleation in NM II-B–depleted cells following expression of the proteins shown. (Scale bar: 40 μm.)

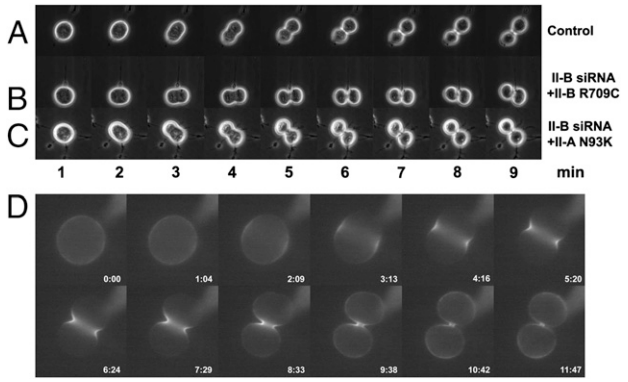

Fig. 2. Time-lapse micrographs of COS-7 cells undergoing cytokinesis. (*A–C*) Phase-contrast microscope images of dividing COS-7 cells from control (*A*) and NMHC II-B siRNA-treated cells expressing either GFP-NM II-B R709C (*B*) or GFP-NM II-A N93K (*C*) show that COS-7 cells expressing a motor-impaired NM II-A and II-B complete cytokinesis no differently than control cells. (*D*) Serial epifluorescence microscope images of GFP-NM II-B R709C show mutant NM II-B R709C driving contractile ring constriction in COS-7 cells following NMHC II-B siRNA treatment.

Two mechanistically different types of cytokinesis (type A and type B) have been reported on the basis of their dependence on or independence of NM II, respectively (12). Type B cytokinesis was initially observed in NM II-deficient *Dictyostelium discoideum*. In contrast to type A, type B cytokinesis relies on cell-matrix adhesion and not contractile ring-dependent equatorial furrowing. To examine whether COS-7 cells expressing only a mutant NM II divide using type A or type B cytokinesis, cell division was analyzed using time-lapse microscopy. The results show that following treatment with NMHC II-B siRNA, COS-7 cells expressing the transfected mutant NM II-A or II-B complete cytokinesis using contractile ring constriction, indicating that these cells use type A cytokinesis despite the presence of a motor-impaired NM II (Fig. 2 *B* anad *C*). Similar to wild-type COS-7 cells undergoing cytokinesis, cells expressing mutant NM II round up and divide into two daughter cells with no obvious evidence of traction-based cytokinesis and then flatten and reattach to the culture surface. No difference in the progression or timing of cell division is found in cells expressing the mutant NM II compared with wild-type cells (Fig. 2 *A–C*). Real-time monitoring of GFP-NM II-B R709C demonstrates the dynamic recruitment of mutant NM II to the cleavage furrow and the mutant NM II-mediated contractile ring constriction in cytokinesis (Fig. 2*D*). Our data suggest that NM II is essential for cytokinesis, but its role in cytokinesis does not appear to depend on its ability to effect actin-filament translocation.

Strong Binding of NM II to Actin Is Required for Cytokinesis. Formation of the actin contractile ring at the equatorial furrow is essential for cytokinesis. Previously, it was reported that ablation of NM II expression disrupted actin filament formation (7, 13), although it has also been reported that early equatorial recruitment of actin is independent of myosin (14). Fig. S1 shows a normal accumulation of F-actin at the equatorial furrow during the progression of cytokinesis in control cells (Fig. S1 *A–C*) as well as in NM II-B–depleted cells (Fig. S1 *D–F*). These results indicate that the failure in cytokinesis following NM II-B ablation is not in formation and maintenance of the actin contractile ring.

It has also been reported that blebbistatin inhibits cleavage furrow formation without disrupting contractile ring assembly in HeLa cells (15). We therefore treated COS-7 cells with different concentrations of blebbistatin (Fig. 3). At 25 μM of blebbistatin, COS-7 cells initiate but cannot complete cleavage furrow formation (Fig. 3*B*). At 50 μM of blebbistatin, COS-7 cells fail to initiate furrow formation (Fig. 3*C*) as previously reported for HeLa cells. Thus, both the ablation of NM II and inhibition of NM II activity by blebbistatin show similar inhibitory effects on cytokinesis in COS-7 cells and indicate that NM II is essential for cytokinesis. Interestingly, inhibition of NM II activity by blebbistatin prevents cytokinesis whereas expression of motor-impaired mutant NM IIs supports cytokinesis. This difference can be attributed to the mechanistic differences in NM II motor inhibition resulting from blebbistatin compared with the NM II mutation: blebbistatin inhibits phosphate release from the myosin–ADP–Pi complex and thereby blocks myosin heads in a product complex with low affinity for actin (i.e., blebbistatin keeps NM II in a weakly actin-bound state and prevents NM II entry into a strong actin-bound, myosin-ADP state) (16). In contrast, NM II-B R709C binds strongly to actin (9, 17). To further understand the importance of NM II binding to actin in cytokinesis, the inhibitory effect of blebbistatin in COS-7 cells that express mutant forms of NM II was investigated. Similar to wild-type COS-7 cells, blebbistatin also arrests cytokinesis in COS-7 cells expressing either NM II-B R709C or NM II-A N93K (Fig. S2). Additional studies using various dosages of blebbistatin at 1, 2, 5, 10, and 20 μM show that COS-7 cells expressing mutant NM II-B R709C have no change in sensitivity to blebbistatin inhibition compared with wild-type COS-7 cells (Table S2). The importance of NM II binding to actin during cytokinesis is also illustrated by the failure of mutant NM II-A Y277F to rescue cytokinesis in NM II-B–depleted COS-7 cells (Fig. S3). This mutant, in contrast to NM-II-A N93K or NM II-B R709C, is defective in binding to actin filaments (18).

Amount of NM II Limits Contractile Ring Constriction. NM II functions by binding to actin to either exert tension on actin filaments or translocate actin filaments (19, 20). Because mutant NM IIs that can bind to actin are unable to translocate actin filaments in vitro, but are still capable of supporting cytokinesis, it is possible that the role of NM II in cytokinesis depends on its ability to generate tension. To further test this hypothesis, cytokinesis in

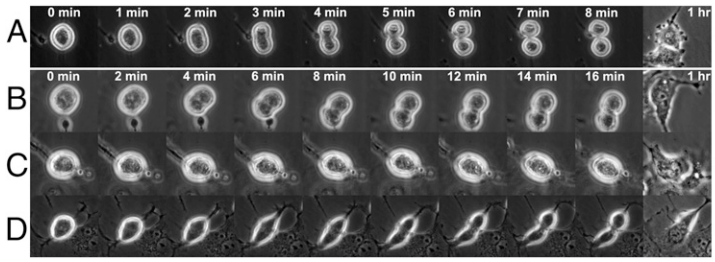

Fig. 3. Blebbistatin inhibition of COS-7 cell cytokinesis. (*A–D*) Time-lapse phase-contrast micrographs of dividing COS-7 cells show that COS-7 cells treated with 25 μM blebbistatin initiate equatorial furrowing but fail to complete cell division (*B*) and that cells treated with 50 μM blebbistatin show no furrowing at all (*C*). *A* and *D* show cytokinesis from an untreated cell (*A*) and NMHC II-B siRNA-treated cell (*D*). The time interval between each panel is 1 min for *A* and 2 min for *B–D*, except for the last panels in each row, which are captured 1 h after the first panels.

COS-7 cells was investigated by graded knockdown of NMHC II-B using three different amounts of siRNA. Following 72 h of treatment with 40, 80, and 200 pmol NMHC II-B siRNA per electroporation, the expression of NM II-B protein in COS-7 cells decreases to 34 ± 10%, 21 ± 6%, and 12 ± 5% of the wild-type cell-expression level, respectively (Fig. 4*A* and Table S3). The number of multinucleated cells increases to 19 ± 6% ($P > 0.05$), 49 ± 8% ($P < 0.01$), and 72 ± 9% ($P < 0.01$), respectively, compared with 14 ± 5% in control cells ($n = 4$ different experiments). Therefore, normal COS-7 cell cytokinesis is NM II-B dose-dependent. To understand how the graded lowering of NM II-B affects cytokinesis in COS-7 cells, the progression of cytokinesis was recorded using time-lapse microscopy 72 h after siRNA treatment. No significant difference is seen between 40 pmol siRNA-treated cells and control cells. At both 80 and 200 pmol of siRNA, ingression of the cleavage furrow is observed, but progression is markedly slower compared with control cells. In both control and NM II-B knockdown cells, the contractile ring constricts at a constant rate during the first ~250 s until late in cytokinesis. The average calculated rate of constriction for control COS-7 cells is 54 ± 12 nm/s ($n = 24$). The average rates for cells treated with 40, 80, and 200 pmol siRNA NM II-B are 44 ± 11 nm/s ($n = 12$), 26 ± 10 nm/s ($n = 12$), and 14 ± 7 nm/s ($n = 22$), respectively. Statistical analysis shows no significant difference between the 40-pmol siRNA-treated and control cells ($P > 0.05$). The 200-pmol transfected cells constrict significantly more slowly than the 80-pmol treated cells ($P < 0.01$), and the latter rate, in turn, is significantly slower than in control cells ($P < 0.01$). These data indicate that the rate of contractile ring constriction is dependent on the amount of NM II-B. The more NM II-B expressed, the faster the ring constricts (Table S3). Recently, a similar finding for myosin II dose dependency was also reported in the cell size-dependent rate of contractile ring constriction of *Neurospora crassa* cells (21). These results are consistent with a role for NM II-B in generating tension to support contractile ring constriction during cytokinesis.

In addition to slowed constriction, many COS-7 cells fail to complete ingression after treatment with 80 and 200 pmol NMHC II-B siRNA, which is consistent with the findings of increased numbers of multinucleated cells in both groups. Because individual cells vary in size, the extent of ring constriction was evaluated as a percentage relative to the initial ring size. As shown in Fig. 4*B*, control COS-7 cells complete 85% of ring constriction within 360 s (Movie S1). (At later stages of cytokinesis, the ring size could not be measured accurately.) The 80 and 200 pmol NMHC II-B siRNA-treated cells complete only about 50 and 30% of ring constriction, respectively, during this same period. The contractile ring in these cells then appears to fluctuate and shows very slow constriction, which is most obvious in cells treated with 200 pmol siRNA (Movie S2). Finally, many cells became binucleated without showing obvious contractile ring regression. These results further support a role for NM II-B in generating tension to complete cytokinesis. Thus, siRNA knockdown of NM

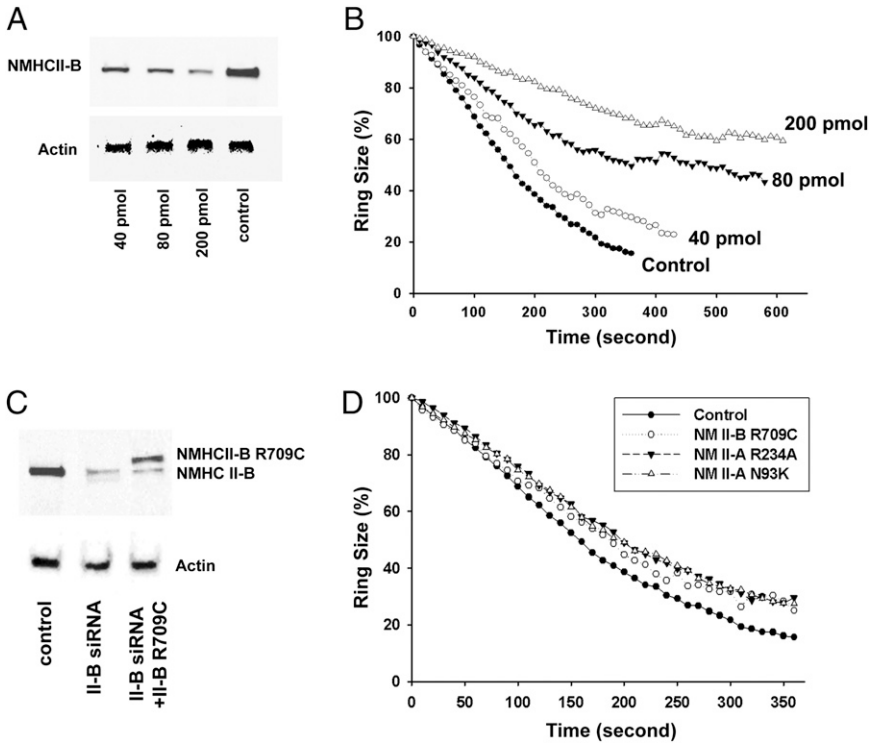

Fig. 4. Loss and restoration of cytokinesis following graded reduction of NM II-B. (*A*) Immunoblot analysis showing graded knockdown of NMHC II-B after 72 h using 40, 80, and 200 pmol of NMHC II-B siRNA. Actin serves as a loading control. (*B*) Size of the contractile ring is depicted as a percentage of initial size (12–24 cells measured). Rate of ring constriction was calculated from the early linear phase. (*C*) Immunoblot showing expression of mutant NMHC II-B R709C in COS-7 cells after transfection with 200 pmol NMHC II-B siRNA. The amount of remaining endogenous NMHC II-B is unchanged following transfection with mutant GFP-NM II-B compared with NMHC II-B siRNA-treated cells. Average expression levels of NMHC II-B R709C and endogenous NMHC II-B are 55 ± 13% ($n = 4$) and 11 ± 2% ($n = 4$), respectively, compared with the wild-type cells. (*D*) Time course of contractile ring size (percentage of the initial size) showing restoration of contractile ring constriction following expression of motor-impaired NM IIs in NMHC II-B siRNA-treated COS-7 cells.

II-B limits tension generation until the furrow is unable to overcome the increasing resistance that occurs at later times of furrow ingression (22). Ultimately, this leads to a failure in cytokinesis. Consistent with our hypothesis, by measuring the traction tension at the cleavage furrow during fibroblast cell division, Burton and Taylor found an increase in force generation at the equatorial furrow during the progression of cytokinesis (23).

To further test our hypothesis, NMHC II-B siRNA knockdown COS-7 cells were transfected with motor-impaired forms of NM II to see if these motor-impaired forms could increase the rate of contractile ring constriction. Fig. 4*C* shows that, although endogenous NMHC II-B levels remain low (11 ± 2% of wild-type level), the exogenous GFP-NMHC II-B R709C is expressed. Time-lapse analyses show that the average rates of contractile ring constriction were 43 ± 6 nm/s (n = 8) and 43 ± 11 nm/s (n = 16) for cells expressing the mutants NM II-B R709C and NM II-A N93K, respectively, in contrast to 14 ± 7 nm/s for cells treated with 200 pmol NMHC II-B siRNA and 54 ± 12 nm/s for control wild-type cells. We also made use of another mutant, NM II-A R234A. This NM II mutation is homologous to a mutation in smooth muscle and skeletal muscle myosin II that abolishes myosin MgATPase activity and in vitro motility on actin filaments (24, 25). Expression of NM II-A R234A also restores the rate of ring constriction in COS-7 depleted of NM II-B (42 ± 11 nm/s vs. 14 ± 7 nm/s in 200 pmol of NM II-B siRNA-treated cells). To test whether small amounts of wild-type NM II-B (10%) could significantly alter the motor activity of mutant NM II-B, the in vitro motility of a mixture of 10% NM II-B wild-type and 90% NM II-B R709C was measured, and no detectable translocation of actin filaments was found (Table S1). Thus, all three mutant NM IIs successfully support cytokinesis and significantly restore the rate of contractile ring constriction (Fig. 4*D*), even though the mutant NM IIs are incapable of translocating actin filaments.

NM II Is Required to Maintain Cortical Stability During Cytokinesis. In addition to the slow and incomplete constriction of the contractile ring in NM II-B siRNA-treated COS-7 cells, the cortical surface of these cells appears to fluctuate during cytokinesis (Movie S2). This cortical fluctuation is not normally seen in control cells (Movie S1). The dynamics of the cortical surface is better illustrated using kymograph analyses (Fig. 5). In control COS-7 cells, the cortical surface appears to be stable during the time period of cytokinesis (Fig. 5*A*). In contrast, the cortical surface of NM II-B siRNA-treated cells is unstable during this time (Fig. 5*B*). Expression of NM II-B R709C (Fig. 5*C*) or NM II-A N93K (Fig. 5*D*) in NM II-B siRNA-treated cells restores stability to the cortical surface. Fig. 5*E* shows a static image of a whole cell as well as the location of the region of interest used to make the kymograph. These results further support the idea that NM II is required to generate cortical tension and maintain the cortical stability of the cell during cytokinesis. Again, this property does not depend on NM II to translocate actin; rather, it depends on its ability to bind and exert tension on actin filaments.

Kinetics of Mutant NM II-B R709C Favor Tension Generation. We used baculovirus-expressed HMM fragments of wild-type and mutant NM II to characterize the kinetic properties of NM II heads. A distinctive property of NM II-B is its unusually high affinity for ADP and prolonged time spent bound to actin filaments in a strongly bound state, resulting in an elevated actin-attachment ratio (duty cycle) (26–29). These features make NM II-B a good candidate for tension generation. By exploiting the intramolecular strain generated in myosin when attached to actin via both heads, it was previously shown that both NM II-A and NM II-B exhibit a marked increase (5- and 12-fold, respectively) in their affinities for ADP under a resistant load (30). This potentiates tension generation by filaments of two-headed myosin strongly attached to actin filaments, which, in turn, may resist actin-filament translocation in the direction opposing that driven by myosin. It has previously been shown that mutant HMM II-B R709C exhibits a very high affinity

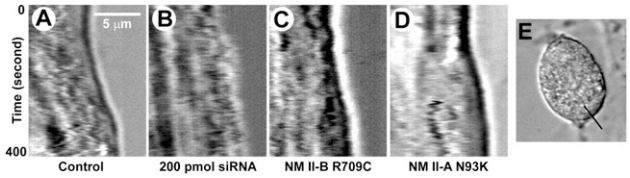

Fig. 5. Cortical membrane instability in dividing COS-7 cells following NM II-B depletion. (*A–D*) Kymograph analysis at a line vertical to the cortical membrane in the polar area of dividing COS-7 cells shows a stable cortical membrane manifested by a smooth progression of the cortical surface during cytokinesis in a control cell (*A*). The cortical surface fluctuates roughly in COS-7 cells treated with NM II-B siRNA (*B*). Expression of mutant NM II-B R709C (*C*) and NM II-A N93K (*D*) restores cortical stability in NM II-B siRNA-treated COS-7 cells. (*E*) A static image of the control cell. The black line indicates the location of the region of interest (ROI) used to make the kymograph. A similar ROI was used for cells imaged in *B–D*.

for ADP when bound to actin and fails to propel actin filaments in the in vitro actin-gliding assay (9). To mimic the in vivo environment, the mechanochemical properties of HMM II-B R709C were investigated in transient kinetic experiments under loaded conditions (Fig. S4). Both ATP chase (Fig. S4*A*) and ADP chase (Fig. S4*B*) traces show a marked decrease in the rate constant of 3′-(N-methylanthraniloyl)-2′-deoxy-ADP (mdADP) release from actin-ADP-NM II-B R709C heads compared with wild-type NM II-B heads. Analysis of ATP-induced dissociation of pyrene actin also shows a marked decrease in the rate constant of ADP release from acto-myosin heads for NM II-B R709C compared with wild-type NM II-B (Fig. S4*C*). Compared with wild-type NM II-B, the affinity of NM II-B R709C for ADP increases 25- and 5-fold at assisting (when force acts in the direction of the myosin power stroke) and resisting (when force acts in the opposite direction) loads, respectively (Table 1). NM II-B R709C heads under a resisting load exhibit very slow ADP release, resulting in extremely long lifetimes of strong actin attachment during steady-state cycling (Fig. S4*D*; note the logarithmic time scale). The calculated mean lifetime that ADP-bound NM II-B R709C heads spend bound to actin reaches 196 s at the resisting load; in contrast, this number is only 43 s for wild-type NM II-B. Thus, the number of actin attachment–detachment cycles during the entire period of cytokinesis in COS-7 cells (~360 s) appears very limited in cells expressing NM II-B R709C. Furthermore, prolonged actin attachment favors the simultaneous attachment of both NM II-B heads to actin and consequently increases tension generation but resists translocation of actin in the opposing direction. This means that NM II-B R709C molecules will rarely detach from actin filaments and that actin will not be translocated due to the slow ATPase cycling. These results argue strongly against a role for NM II-B R709C in translocating actin filaments during cytokinesis. The role of NM II in generating tension applies to both NM II-A and NM II-B, which, because of their unique load-dependent kinetics, differ from skeletal muscle myosin (30).

Motor-Impaired NM II Supports Cytokinesis During Mouse Development. Cells in 2D culture often behave differently compared with cells in vivo in a 3D environment, which imposes a different set of geometric constraints on the dividing cell. Moreover, cultured COS-7 cells treated with NM II-B siRNA always contain a small amount of residual endogenous wild-type myosin. To test whether motor-impaired NM II could also support cytokinesis in vivo during mouse development in the complete absence of wild-type NM II, we made use of NM II-A and II-B genetically altered mouse lines. In NM II-A ablated mice, the visceral endoderm of the early embryo [embryonic day 6.5 (E6.5)] shows marked evidence for a defect in cytokinesis, including multinucleation and malformed nuclei (compare Fig. S5*E* with S5*D*, wild type). This defect can be rescued by replacing wild-type NM II-A with a mutant form of NM II-A, R702C (the homolog of R709C II-B), which rescues cytokinesis (compare Fig. S5*B* with S5*A*) but cannot support

Table 1. Kinetics of nucleotide binding to and dissociation from actin-bound NM II HMM

HMM construct	ATP binding* k_{on} ($\mu M^{-1}s^{-1}$) (+ actin)	ADP binding† k_{on} ($\mu M^{-1}s^{-1}$) (+ actin)	ADP release		
			$k_+(s^{-1})^{*,\ddagger}$ (assisting load)	$k_0(s^{-1})^*$ (unloaded)	$k_-(s^{-1})^{\ddagger}$ (resisting load)
NM II-A wt[§]	0.23 ± 0.03	3.4 ± 0.1	11 ± 4	2.9 ± 1.0	0.59 ± 0.09
NM II-B wt[§]	0.25 ± 0.09	3.1 ± 0.1	1.1 ± 0.3	0.27 ± 0.06	0.023 ± 0.003
NM II-B R709C	0.34 ± 0.03	1.8 ± 0.1[¶]	0.044 ± 0.003	0.014 ± 0.002	0.0051 ± 0.0019

Parameters were measured as described earlier for wild-type NM II constructs (ref. 30; see also Fig. S4). Means ± SEM are shown for values obtained in all experiments using 3′-(N-methylanthraniloyl)-2′-deoxy-ADP (mdADP) and pyrene-actin signals (*n* was between 3 and 10).
*From pyrene-actin fluorescence data (Fig. S4*C*).
†From mdADP fluorescence data (trace not shown).
‡From mdADP fluorescence (ADP chase) data (Fig. S4*B*).
§From ref. 30.
¶From ref. 9.

normal placenta development, showing that the mutant myosin is defective in certain cell functions (31).

We next examined cardiac myocyte cytokinesis in mice expressing NM II-B R709C in place of wild-type NM II-B. Previous experiments using genetically altered mice have demonstrated that mice ablated for NM II-B (B^-/B^-) or expressing a reduced amount of NM II-B R709C show an abnormal accumulation of binucleated cardiac myocytes in embryonic hearts [25–30% compared with 1–5% for wild type (Fig. 6*B*)] (32). We refer to the mutant hypomorphic mice as B^{CN}/B^{CN} mice, where C represents the R-to-C mutation, and N represents the neomycin^r cassette. Surprisingly, increasing mutant NM II-B R709C expression to wild-type levels by removing the floxed neomycin^r cassette in B^C/B^C mouse hearts prevents binucleation [<1%, 14 of 1,888 cardiac myocytes counted, $n = 6$ mice (Fig. 6*C*)], despite the fact that the mutant NM II-B cannot translocate actin in an in vitro motility assay under unloaded conditions (Table S1) (9). This suggests that the defect in cytokinesis in B^{CN}/B^{CN}, similar to that in B^-/B^- cardiac myocytes, was due to a decrease in the overall NM II content, rather than to the presence of the mutant NM II-B. Although NM II-B R709C rescues the defect in cytokinesis in cardiac myocytes, it fails to support normal heart development in B^C/B^C mice, which have a strikingly thinner compact myocardium (Fig. 6*C*) compared with B^+/B^+ mice (Fig. 6*A*), confirming that NM II-B R709C is a defective motor in vivo. Moreover, the mutant NM II-B causes numerous other abnormalities, including defects in neuronal migration (11). These findings in the context of a 3D environment lend further support to the hypothesis that mutant NM II under loaded conditions can support cytokinesis by exerting tension rather than by actin translocation.

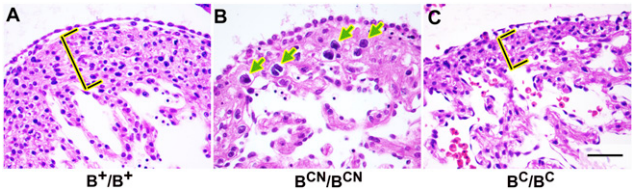

Fig. 6. Mutant NM II-B supports cytokinesis in mouse cardiomyocytes in vivo. (*A*–*C*) H&E-stained heart sections from E14.5 embryos. *B* shows bi- or multinucleated cardiomyocytes in a hypomorphic B^{CN}/B^{CN} heart (arrows) in contrast to a B^+/B^+ heart (*A*). Hypomorphism is eliminated by removing the neomycin^r cassette to generate B^C/B^C mice expressing wild-type quantities of mutant NM II-B. Fewer than 1% binucleated myocytes were found in mutant B^C/B^C hearts (*C*). The compact myocardium in B^C/B^C embryos (*C*, bracket) is significantly thinner compared with that of B^+/B^+ embryos (*A*, bracket), reflecting the defective NM II-B R709C motor in vivo despite rescue of cytokinesis. (Scale: 150 μm.)

Discussion

We have previously demonstrated that the mutant NM II-B R709C can support cell–cell adhesion at the apical surface of the developing mouse neuroepithelial cells bordering the spinal canal, despite its inability to translocate actin filaments in an in vitro motility assay and its compromised MgATPase activity (11). The results presented here support the role of NM II to bind and cross-link actin and exert tension on actin during cytokinesis. The contribution of NM II to tension generation in cytokinesis has also been proposed in previous reports. For example, NM II provides the major cortical tension to counteract the increasing hydrostatic pressure during mitotic cell rounding (33). During *Dictyostelium discoideum* cytokinesis, NM II is the major contributor to active tension in addition to surface tension (34). However, on an adhesive surface, unlike mouse cardiac myocytes and COS-7 cells, *D. discoideum* could still undergo cytokinesis even in the absence of NM II (35, 36). The function of NM II to generate tension is also consistent with the results from fission yeast where a mutant myosin II exhibiting only 2% of wild-type motile activity could support fission yeast cytokinesis (37). Studies from myosin II null *D. discoideum* complemented with 10-fold slower myosin II S456L also concluded that the velocity of the myosin motor is not rate limiting for furrow ingression (38). In addition to generating tension during cytokinesis, NM II can also act to accelerate actin filament turnover (39–42), thereby remodeling and reshaping the contractile ring.

Motor-independent contraction via cytoskeleton cross-linking has been proposed to drive cytokinesis in different organisms, including bacteria, *Saccharomyces cerevisiae*, and *D. discoideum* (43). However, these organisms either expressed no NM II or NM II was genetically ablated. In both COS-7 cells in culture and cardiac myocytes in developing mouse hearts, ablation of NM II resulted in a failure of cytokinesis. Thus, other molecular motors and/or cross-linking proteins are not sufficient to effect cytokinesis in these cells. Although the motor-impaired NM II-B R709C fails to propel actin filaments in vitro and fails to support normal heart development in mice, it supports cytokinesis in both COS-7 cells and cardiac myocytes similarly to wild-type NM II-B.

The molecular mechanism that explains how NM II cross-linking drives cytokinesis remains unclear. Results from this report show that this mechanism is not dependent on the ability of myosin to translocate actin filaments, but that NM II binding to actin helps support cortical tension during cytokinesis. Our results thus suggest that in vertebrate cells NM II is required not for its motor activity to translocate actin, but for its cross-linking activity to generate the tension that drives cytokinesis. Generation of tension by NM II-B in COS-7 cytokinesis is essential especially at the initiation of ring constriction. Both ablation of NM II-B and blebbistatin treatment stop contractile ring constriction. The mechanosensitive behavior of NM II supports the following model of NM II in cytokinesis: During contractile ring constriction, the resisting load enhances the capability of NM II to generate tension by increasing its duty ratio

and cross-linking of actin filaments, which helps to initiate ring constriction. The constriction of the ring, in turn, generates an assisting load to the myosin head that helps NM II to detach from actin and reshape the ring, without hampering the progression of ring constriction. These important load-dependent properties of NM IIs make it possible for NM IIs to play a critical role in vertebrate cytokinesis without translocating actin filaments.

Materials and Methods

Nonmuscle Myosin II Mutant Mice. NMHC II-B R709C mutant mice (B^{CN}/B^{CN} and B^{C}/B^{C} mice) were generated as previously described (11). NMHC II-A R702C mutant mice (A^{C}/A^{C} mice) were generated as previously described (31). All procedures were conducted using an approved animal protocol in accordance with the National Heart, Lung, and Blood Institute Animal Care and Use Committee protocols. B^{CN}/B^{CN} (ID 16142) and B^{C}/B^{C} (ID 16983) mice are available from the Mutant Mouse Regional Resource Centers (http://www.mmrrc.org).

Time-Lapse Analysis. Time-lapse analysis was carried out using an inverted microscope (Olympus IX-70) equipped with a custom environmental chamber with 5% CO_2 at 37 °C. For detailed analysis of cytokinesis, images were captured at 2-s intervals using an Olympus live-cell imaging system (Olympus VivaView). National Institutes of Health ImageJ was used to measure the contractile ring size.

Kinetic Measurements. Experiments were performed using KinTek SF-2001 and SF-2004 apparatuses at 25 °C in a buffer containing 10 mM 4-morpholinepropanesulfonic acid (pH 7.0), 2 mM $MgCl_2$, 0.15 mM EGTA, and 100 mM KCl. In experiments starting from nucleotide-free acto-HMM, the proteins were preincubated with 0.01 units/mL apyrase for 30 min at 25 °C to remove ATP and ADP contamination.

Detailed methods and materials can be found in *SI Materials and Methods*.

ACKNOWLEDGMENTS. We thank Dr. Dennis E. Discher (University of Pennsylvania) for providing the plasmid NMHC II-B Y277F; and Dr. Edward Korn (Laboratory of Cell Biology, National Heart, Lung, and Blood Institute), Dr. Sachiyo Kawamoto, and members of the Laboratory of Molecular Cardiology for critical comments on the manuscript. We also thank Dr. Douglas Robinson (The Johns Hopkins University School of Medicine) for his expertise in the analysis of the dynamics of cytokinesis; Dr. Jianjun Bao for help with COS-7 experiments; Drs. Chengyu Liu and Yubin Du (National Heart, Lung, and Blood Institute Transgenic Core); and Drs. Christian A. Combs and Daniela Malide (National Heart, Lung, and Blood Institute Light Microscopy Core) for professional skills and advice. Antoine Smith and Dalton Saunders provided excellent technical assistance. This research was supported by the Division of Intramural Research, National Heart, Lung, and Blood Institute. M.K. is a Bolyai Fellow of the Hungarian Academy of Sciences and is funded by Norway Grant NNF2-85613, the Hungarian Scientific Research Fund (K71915 and NK81950), Társadalmi Megújulás Operatív Program Grant 4.2.1/B-09/1/KMR-2010-0003, and the "Momentum" Program of the Hungarian Academy of Sciences (LP2011-006/2011).

1. Conti MA, Kawamoto S, Adelstein RS (2008) Non-muscle myosin II. *Myosins: A Superfamily of Molecular Motors (Proteins and Cell Regulation)*, ed L. M. Coluccio (Springer, Berlin; Heidelberg; London; New York), pp 223–264.
2. Bohnert KA, Gould KL (2011) On the cutting edge: Post-translational modifications in cytokinesis. *Trends Cell Biol* 21:283–292.
3. Glotzer M (2005) The molecular requirements for cytokinesis. *Science* 307:1735–1739.
4. Matsumura F (2005) Regulation of myosin II during cytokinesis in higher eukaryotes. *Trends Cell Biol* 15:371–377.
5. Noguchi T, Arai R, Motegi F, Nakano K, Mabuchi I (2001) Contractile ring formation in Xenopus egg and fission yeast. *Cell Struct Funct* 26:545–554.
6. Pollard TD (2010) Mechanics of cytokinesis in eukaryotes. *Curr Opin Cell Biol* 22(1): 50–56.
7. Bao J, Jana SS, Adelstein RS (2005) Vertebrate nonmuscle myosin II isoforms rescue small interfering RNA-induced defects in COS-7 cell cytokinesis. *J Biol Chem* 280: 19594–19599.
8. Hu A, Wang F, Sellers JR (2002) Mutations in human nonmuscle myosin IIA found in patients with May-Hegglin anomaly and Fechtner syndrome result in impaired enzymatic function. *J Biol Chem* 277:46512–46517.
9. Kim KY, Kovács M, Kawamoto S, Sellers JR, Adelstein RS (2005) Disease-associated mutations and alternative splicing alter the enzymatic and motile activity of nonmuscle myosins II-B and II-C. *J Biol Chem* 280:22769–22775.
10. Seri M, et al. (2003) MYH9-related disease: May-Hegglin anomaly, Sebastian syndrome, Fechtner syndrome, and Epstein syndrome are not distinct entities but represent a variable expression of a single illness. *Medicine (Baltimore)* 82:203–215.
11. Ma X, Bao J, Adelstein RS (2007) Loss of cell adhesion causes hydrocephalus in nonmuscle myosin II-B-ablated and mutated mice. *Mol Biol Cell* 18:2305–2312.
12. Kanada M, Nagasaki A, Uyeda TQ (2005) Adhesion-dependent and contractile ring-independent equatorial furrowing during cytokinesis in mammalian cells. *Mol Biol Cell* 16:3865–3872.
13. Goeckeler ZM, Bridgman PC, Wysolmerski RB (2008) Nonmuscle myosin II is responsible for maintaining endothelial cell basal tone and stress fiber integrity. *Am J Physiol Cell Physiol* 295:C994–C1006.
14. Zhou M, Wang YL (2008) Distinct pathways for the early recruitment of myosin II and actin to the cytokinetic furrow. *Mol Biol Cell* 19:318–326.
15. Straight AF, et al. (2003) Dissecting temporal and spatial control of cytokinesis with a myosin II Inhibitor. *Science* 299:1743–1747.
16. Kovács M, Tóth J, Hetényi C, Málnási-Csizmadia A, Sellers JR (2004) Mechanism of blebbistatin inhibition of myosin II. *J Biol Chem* 279:35557–35563.
17. Vicente-Manzanares M, Zareno J, Whitmore L, Choi CK, Horwitz AF (2007) Regulation of protrusion, adhesion dynamics, and polarity by myosins IIA and IIB in migrating cells. *J Cell Biol* 176:573–580.
18. Shin JW, Swift J, Spinler KR, Discher DE (2011) Myosin-II inhibition and soft 2D matrix maximize multinucleation and cellular projections typical of platelet-producing megakaryocytes. *Proc Natl Acad Sci USA* 108:11458–11463.
19. Conti MA, Adelstein RS (2008) Nonmuscle myosin II moves in new directions. *J Cell Sci* 121(1):11–18.
20. Vicente-Manzanares M, Ma X, Adelstein RS, Horwitz AR (2009) Non-muscle myosin II takes centre stage in cell adhesion and migration. *Nat Rev Mol Cell Biol* 10:778–790.
21. Calvert ME, et al. (2011) Myosin concentration underlies cell size-dependent scalability of actomyosin ring constriction. *J Cell Biol* 195:799–813.
22. Matzke R, Jacobson K, Radmacher M (2001) Direct, high-resolution measurement of furrow stiffening during division of adherent cells. *Nat Cell Biol* 3:607–610.
23. Burton K, Taylor DL (1997) Traction forces of cytokinesis measured with optically modified elastic substrata. *Nature* 385:450–454.
24. Onishi H, Morales MF, Kojima S, Katoh K, Fujiwara K (1998) Smooth muscle myosin. Amino acid residues responsible for the hydrolysis of ATP. *Adv Exp Med Biol* 453: 99–103; discussion 103–104.
25. Shimada T, Sasaki N, Ohkura R, Sutoh K (1997) Alanine scanning mutagenesis of the switch I region in the ATPase site of Dictyostelium discoideum myosin II. *Biochemistry* 36:14037–14043.
26. Norstrom MF, Smithback PA, Rock RS (2010) Unconventional processive mechanics of non-muscle myosin IIB. *J Biol Chem* 285:26326–26334.
27. Kovács M, Wang F, Hu A, Zhang Y, Sellers JR (2003) Functional divergence of human cytoplasmic myosin II: Kinetic characterization of the non-muscle IIA isoform. *J Biol Chem* 278:38132–38140.
28. Wang F, et al. (2003) Kinetic mechanism of non-muscle myosin IIB: Functional adaptations for tension generation and maintenance. *J Biol Chem* 278:27439–27448.
29. Rosenfeld SS, Xing J, Chen LQ, Sweeney HL (2003) Myosin IIb is unconventionally conventional. *J Biol Chem* 278:27449–27455.
30. Kovács M, Thirumurugan K, Knight PJ, Sellers JR (2007) Load-dependent mechanism of nonmuscle myosin 2. *Proc Natl Acad Sci USA* 104:9994–9999.
31. Zhang Y, et al. (2012) Mouse models of MYH9-related disease: Mutations in nonmuscle myosin II-A. *Blood* 119:238–250.
32. Takeda K, Kishi H, Ma X, Yu ZX, Adelstein RS (2003) Ablation and mutation of nonmuscle myosin heavy chain II-B results in a defect in cardiac myocyte cytokinesis. *Circ Res* 93:330–337.
33. Stewart MP, et al. (2011) Hydrostatic pressure and the actomyosin cortex drive mitotic cell rounding. *Nature* 469:226–230.
34. Zhang W, Robinson DN (2005) Balance of actively generated contractile and resistive forces controls cytokinesis dynamics. *Proc Natl Acad Sci USA* 102:7186–7191.
35. Neujahr R, Heizer C, Gerisch G (1997) Myosin II-independent processes in mitotic cells of Dictyostelium discoideum: Redistribution of the nuclei, re-arrangement of the actin system and formation of the cleavage furrow. *J Cell Sci* 110(2):123–137.
36. Zang JH, et al. (1997) On the role of myosin-II in cytokinesis: Division of Dictyostelium cells under adhesive and nonadhesive conditions. *Mol Biol Cell* 8:2617–2629.
37. Lord M, Pollard TD (2004) UCS protein Rng3p activates actin filament gliding by fission yeast myosin-II. *J Cell Biol* 167:315–325.
38. Reichl EM, et al. (2008) Interactions between myosin and actin crosslinkers control cytokinesis contractility dynamics and mechanics. *Curr Biol* 18:471–480.
39. Haviv L, Gillo D, Backouche F, Bernheim-Groswasser A (2008) A cytoskeletal demolition worker: Myosin II acts as an actin depolymerization agent. *J Mol Biol* 375: 325–330.
40. Guha M, Zhou M, Wang YL (2005) Cortical actin turnover during cytokinesis requires myosin II. *Curr Biol* 15:732–736.
41. Murthy K, Wadsworth P (2005) Myosin-II-dependent localization and dynamics of F-actin during cytokinesis. *Curr Biol* 15:724–731.
42. Medeiros NA, Burnette DT, Forscher P (2006) Myosin II functions in actin-bundle turnover in neuronal growth cones. *Nat Cell Biol* 8:215–226.
43. Sun SX, Walcott S, Wolgemuth CW (2010) Cytoskeletal cross-linking and bundling in motor-independent contraction. *Curr Biol* 20:R649–R654.